LBNL-38887
UC-401
Preprint

ERNEST ORLANDO LAWRENCE
BERKELEY NATIONAL LABORATORY

Technetium Speciation in Cement Waste Forms Determined by X-ray Absorption Fine Structure Spectroscopy

P.G. Allen, G.S. Siemering, D.K. Shuh,
J.J. Bucher, N.M. Edelstein, C.A. Langton,
S.B. Clark, T. Reich, and M.A. Denecke
Chemical Sciences Division

May 1996
Submitted to
Radiochimica Acta

DISCLAIMER

LBNL-38887
UC-401

Technetium Speciation in Cement Waste Forms Determined by X-ray Absorption Fine Structure Spectroscopy

P.G. Allen,[1,2] G.S. Siemering,[1] D.K. Shuh,[1] J.J. Bucher,[1] N.M. Edelstein,[1]
C.A. Langton,[3] S.B. Clark,[4] T. Reich,[5] and M.A. Denecke[5]

[1]Chemical Sciences Division, Ernest Orlando Lawrence Berkeley National Laboratory, Berkeley, CA 94720

[2]G.T. Seaborg Institute for Transactinium Science, Lawrence Livermore National Laboratory, Livermore, CA 94551

[3]Westinghouse Savannah River Company, Savannah River Technology Center, Aiken, SC 29808

[4]Washington State University, Department of Chemistry, Pullman, WA 99164

[5]Forschungszentrum Rossendorf e. V., Institut für Radiochemie, Postfach 51 01 19, D-01314 Dresden, Germany

May 1996

This work was supported by the Director, Office of Energy Research, Office of Basic Energy Sciences, Chemical Sciences Division, of the U.S. Department of Energy under Contract No. DE-AC03-76SF00098, and by Lawrence Livermore National Laboratory under Contract No. W-7405-ENG-48.

Technetium Speciation in Cement Waste Forms Determined by X-ray Absorption Fine Structure Spectroscopy

P. G. Allen,[1,2*] G. S. Siemering,[1] D. K. Shuh,[1] J. J. Bucher,[1] N. M. Edelstein,[1]
C. A. Langton,[3] S. B. Clark,[4] T. Reich,[5] and M. A. Denecke[5]

[1]Chemical Sciences Division, Lawrence Berkeley National Laboratory, Berkeley, CA 94720
[2]G.T. Seaborg Institute for Transactinium Science, Lawrence Livermore National Laboratory, Livermore, CA 94551
[3]Westinghouse Savannah River Company, Savannah River Technology Center, Aiken, SC 29808
[4]Washington State University, Department of Chemistry, Pullman, WA 99164
[5]Forschungszentrum Rossendorf e. V., Institut für Radiochemie, Postfach 51 01 19, D-01314 Dresden, Germany.

Abstract

The chemistry of technetium in cement waste forms has been studied with x-ray absorption fine structure (XAFS) spectroscopy. Using the Tc K-edge x-ray absorption near-edge structure (XANES) as a probe of the technetium speciation, our results show that partial reduction of the pertechnetate ion, TcO_4^-, takes place in the presence of the cement additive, blast furnace slag (BFS). The addition of the reducing agents FeS, Na_2S, and NaH_2PO_2 produces more extensive reduction of TcO_4^-, while the compounds FeO, Fe_3O_4, and Mn_3O_4 are observed to be unreactive. The extended x-ray absorption fine structure (EXAFS) data for the BFS, Na_2S, and FeS treated cements indicate the presence of Tc clusters possessing first shell S coordination. For the Na_2S and FeS additives, Tc–Tc interactions are detected in the EXAFS demonstrating an extended structure similar to that of TcS_2. The EXAFS spectrum of the NaH_2PO_2 treated cement reveals Tc–O and Tc–Tc interactions that resemble those found in the structure of TcO_2.

Keywords: EXAFS, XANES, Cement, Technetium, X-ray
Shortened Title: Technetium Speciation in Cement Waste Forms

Introduction

Cement-based waste forms are an integral component of national strategies being developed for the safe, long-term storage of low and intermediate-level radioactive waste [1-6]. Numerous physical properties of the cement such as strength, porosity, corrosion resistance, and leachability must be evaluated to effectively encapsulate the hazardous species for long periods of time and under a wide range of environmental conditions. Of these properties, leachability is perhaps the most critical in regards to the immobilization of radionuclides in these matrices. ^{99}Tc in particular has received considerable attention due to its abundance in nuclear wastes, relatively long half-life, and the high solubility of its most common, oxidized form, the pertechnetate anion (TcO_4^-).

Because the chemical form or speciation of a radionuclide directly determines many of its properties, modifying the speciation *in-situ* to control solubility and transport is vital for immobilization. In the case of Tc, a decrease in the leaching rate has been achieved through the use of blast furnace slag (BFS) additives to the ordinary Portland cement (OPC) formulations [7, 8]. The decreased leaching of Tc is believed to result from the reduction of TcO_4^- to a less soluble form, i.e. Tc(IV) as in TcO_2, by the presence of reducing agents contained in the BFS such as Fe(II) [7] or sulfur-containing species [8].

We have used x-ray absorption fine structure (XAFS) spectroscopy to determine the Tc speciation induced by the introduction of various chemical additives to the cement formulations. XAFS spectroscopy [9,10] is an element specific structural technique that is typically divided into two methods concentrating on different portions of an x-ray absorption spectrum. The x-ray absorption near edge structure (XANES) region lies within ~20 eV above and below the main absorption edge and provides information about the electronic structure (density of states, oxidation state) and local geometry for a given absorbing atom. The extended x-ray absorption fine structure (EXAFS) region spans the range ~20-1200 eV past the edge and can be used to determine the identity of near-neighbor atoms ($Z \pm 2$-6), their coordination numbers ($N \pm 20\%$), and bond lengths ($R \pm 0.01$Å) [9,10]. XAFS does not require long-range order (i.e., crystalline

samples) and can be performed on elements in amorphous solids, surface complexes, and aqueous species. This is a key point for the study of Tc and other elements in cement. Recently, XAFS was utilized to investigate the speciation of Tc [11] and Cr [12] in cement-based waste forms. In the present study, the XANES region is used as a sensitive measure of the Tc oxidation state, thereby making it possible to quantify the extent of reduction that takes place in the presence of various additives (BFS, FeS, or Na_2S) and under different curing conditions. In addition, the Tc EXAFS is used to identify the local structure of several reduced Tc species in the cement waste forms.

Experimental

Model Compounds. Several Tc and Re models were obtained in order to provide well-characterized XANES and EXAFS spectra to be used as references for the Tc cement spectra. Tc metal was obtained from A. Sattelberger at Los Alamos National Laboratory. NH_4TcO_4 (aq) was purchased from Oak Ridge National Laboratory. TcO_2 [13], NH_4TcOCl_4 [14], and $(NH_4)_2TcCl_6$ [15] were prepared by methods found in the literature using NH_4TcO_4 (aq) as the starting material. In addition, one other Tc compound was obtained from a portion of the TcO_2 synthesis [13]. This material, subsequently referred to as "LiOH-treated," was taken after precipitation of Tc by the addition of LiOH and was in the form of a wet paste. $HReO_4$ (aq) was prepared by dissolving Re_2O_7 into deionized water. ReS_2 was purchased from Alfa Aesar Chemicals and its structure was checked by powder x-ray diffraction (XRD) [16].

Cement Preparations. Three different cement formulations were prepared using various combinations of ordinary Portland cement, blast furnace slag, pulverized fly ash (PFA), and a simulated waste solution (SWS). The preparation details of the SWS have been reported elsewhere [17], and the compositions of cement Mixes 1, 2, and 3 are summarized in Table 1. Approximately 1200 ppm of TcO_4^- was added to each of the three cement formulations in the form of a NH_4TcO_4 stock solution. Separate portions of each Tc/cement mixture were subsequently cured at two different temperatures (20°C and 60°C) and for periods of 1, 7, 15, and 30 days

under 100% humidity. In addition, ~10 wt% FeS was added to some cement mixtures to evaluate its effects under these curing conditions.

A second series of cement mixtures was prepared to examine more closely the effectiveness of the reductants FeS, Na_2S, BFS, FeO, Fe_3O_4, Mn_3O_4, and NaH_2PO_2 in reducing TcO_4^-. In particular, results from this series of reductants should make it possible to discern the role of S and Fe in the BFS. Seven separate samples were prepared with each containing ~10 wt% of a single reductant and 1200 ppm of TcO_4^- added to a 1:1 wt% mixture of SWS/OPC (Mix 1). These samples were cured for 4 days at 60°C under 100% humidity.

XAFS Data Acquisition and Analysis. The TcO_2, NH_4TcOCl_4, and $(NH_4)_2TcCl_6$ samples were mixed with boron nitride (BN) powder so that an edge jump of ~1 was obtained over the Tc K-edge. ReS_2 was diluted with BN and gave a jump of ~0.1 at the Re L_1-edge. These samples, in addition to the LiOH-treated sample (undiluted paste), were mounted in 4 mm thick x-ray transmission cells consisting of a slotted (6 x 25 mm) polyethylene frame with 0.125 mm kapton windows on each side. Solutions of 0.2M NH_4TcO_4 (aq) and 0.3M $HReO_4$ (aq)were sealed in 10 mm diameter plastic NMR tubes and were sufficiently transparent so that data could be acquired in transmission mode. The Tc metal spectrum was collected from 1g of metal particles (~1 mm dia.) also sealed in a 10 mm NMR tube. Since the Tc metal was too thick to measure by x-ray transmission, its spectrum was taken in fluorescence mode using a Ge solid-state detector and subsequently corrected for self-absorption effects [18].

All of the cement samples were cured in polystyrene UV-visible cuvettes (4 x 10 mm body). The cement loaded cuvettes and the cells containing the standards were placed in heat-sealed 0.05 mm polyethylene bags to ensure containment during XAFS data acquisition. The primary polyethylene containers were heat-sealed and surrounded by a second, heat-sealed bag for safety purposes (not used for Re). Using the 4 mm path length from the cuvettes, the final Tc concentration in the cements yielded an edge jump ~0.07 across the Tc K absorption edge (21 keV). At this energy, x-ray attenuation by the polystyrene cuvette was insignificant. The

homogeneity of these solid solutions enabled all XANES and EXAFS data for the cement samples to be measured in transmission mode.

Tc K-edge and Re L_1-edge x-ray absorption spectra were collected at the Stanford Synchrotron Radiation Laboratory (SSRL) on beamlines 4-3, 4-1, and 2-3 (each unfocused) under dedicated ring conditions (3.0 GeV, 50-100 mA) using Si (220) double-crystal monochromators. Rejection of higher order harmonic content of the beam was achieved by detuning the angle between crystals in the monochromator so that the incident flux was reduced to 50% of its maximum. All spectra were collected using a vertical slit aperture of 0.5 mm. Three XAFS scans were collected from each sample at room temperature and the results averaged. The spectra were energy calibrated by simultaneously measuring the spectrum from the 0.2M NH_4TcO_4 (aq) or 0.3M $HReO_4$ (aq) reference solutions which were placed between the second and third ionization chambers. The first inflection point of the pre-edge absorption peak for each reference was defined as 21044 eV and 12527 eV for the Tc K and Re L_1-edges, respectively. XAFS data reduction was performed by standard methods [19] using the EXAFSPAK suite of computer codes developed by G. George of SSRL. XAFS data reduction included pre-edge background subtraction followed by spline fitting and normalization (based on the Victoreen falloff) to extract the EXAFS data above the threshold energy, with E_o defined as 21065 eV (Tc). Curve-fitting analyses were done utilizing EXAFSPAK to fit the raw k^3-weighted EXAFS data. The theoretical EXAFS modeling code, FEFF6, of Rehr et al. [20] was employed to calculate the backscattering phases and amplitudes of the individual neighboring atoms, O, S, Cl, or Tc. FEFF6 calculations were done using parameters from previously determined structures for $KTcO_4$ [21], $(Bu_4N)TcOCl_4$ [22], $(NH_4)_2TcCl_6$ [23], TcO_2 [24], and TcS_2 [25]. The amplitude reduction factor, S_0^2, was held fixed at 0.9 for all of the fits. The shift in threshold energy, ΔE_0, was allowed to vary as a global parameter for all atoms included in the fits (i.e., the same ΔE_0 was used for all the shells).

Results and Discussion

1. XANES.

K and L_1 x-ray absorption edges arise from the excitation of 1s and 2s electrons, respectively, and may display a variety of distinct or overlapping transitions superimposed on the main absorption edge. The most commonly assigned transitions for coordinated transition metals are the s $\rightarrow$ nd, ns, and np final states [26]. Although it is electric dipole forbidden, the s $\rightarrow$ nd transition is frequently observed due to p orbital mixing with the final d state [27]. The intensity of this transition is highly dependent on site symmetry, nearest-neighbor bond lengths, and d-orbital occupancy [26, 28]. In addition, the energies of the s $\rightarrow$ nd, ns, and np transitions and the main absorption edge are dependent on the effective charge of the absorbing atom, ligand electronegativities, bond lengths, and coordination numbers [26].

The Tc K-edge XANES data for the series of Tc model compounds are shown in Figure 1. Apart from differences in the fine structure, a general trend is seen whereby the main absorption edge shifts to higher energies as the valence of the Tc increases. This behavior reflects the increased energy required to ionize the Tc by removal of the 1s electron. The main absorption edges shift ~12 eV [29] upon going from Tc metal to Tc(VII) in NH_4TcO_4 (aq). While most of these compounds exhibit a featureless, smoothly rising absorption edge, some have a pre-edge transition which is particularly apparent in the XANES of NH_4TcOCl_4 and NH_4TcO_4. In analogy to the XANES spectra of first-row transition metals, this feature is assigned to the forbidden 1s $\rightarrow$ 4d transition which becomes more allowed in the noncentrosymmetric, tetrahedral TcO_4^- species [30]. The geometry in $TcOCl_4^-$ is distorted square pyramidal, thus the extent of p orbital mixing is less as shown by the diminished magnitude of the pre-edge peak relative to TcO_4^-. The decreased amplitude of this feature in the TcO_2 and LiOH-treated spectra indicates a further departure from the case of pure tetrahedral geometry, and can also be correlated with longer Tc–O bond lengths in these compounds. Accordingly, $(NH_4)_2TcCl_6$ which contains an ideal octahedral Tc site (center of symmetry) shows no pre-edge absorption feature. The absorption edge of $(NH_4)_2TcCl_6$ is shifted to a lower energy than the TcO_2 edge despite the fact that the Tc atoms in each compound have the

same oxidation state. This reflects the reduced effective charge on the Tc in $TcCl_6^{2-}$ resulting from the greater electron donation of the Cl ligands.

Figure 2 shows a series of representative XANES spectra for (a) TcO_4^- + FeS in Mix 3 cured at 60°C for 15 days; (b) TcO_4^- in Mix 2 cured at 60°C for 7 days; and (c) TcO_4^- in Mix 1 cured at 60°C for 1 day. Moving from (a) to (c), decreased reduction of TcO_4^- is observed. The absence of any pre-edge feature in spectrum (a) indicates that no TcO_4^- or TcO^{3+} (as in $TcOCl_4^-$) is present. In addition, the position of the main absorption edge in spectrum (a) suggests that the Tc species present here is reduced to a similar extent as TcO_2 or $(NH_4)_2TcCl_6$ shown in Figure 1. Spectrum (b) depicts a situation where only partial reduction has occurred. EXAFS curve fitting results described below confirm the presence of residual TcO_4^- (rather than TcO^{3+}) along with a more reduced species. Because it is a mixture, the main edge in (b) is broader than that of TcO_4^-.

Assuming each Tc cement sample is composed of a binary mixture of the reduced and oxidized Tc species in Figures 2(a) and 2(c), we are able to determine the extent of reduction by deconvoluting the normalized Tc XANES data. Figure 2(c) shows the deconvolution for the unreduced sample, demonstrating the separation into features 1 and 2. Based on this model, we can analyze for the reduction of TcO_4^- by fitting two features: 1) the amplitude of the $1s \rightarrow 4d$ transition, which is proportional to the amount of TcO_4^- present; and 2) the shift in the main absorption edge step function relative to that of the TcO_4^- reference spectrum. For feature 2, larger absorption edge shifts to lower energy indicate a more reduced state. The fits were performed with EXAFSPAK, where the pre-edge transition is treated as a pseudo-Voigt peak, and the step function is the integral of a pseudo-Voigt function.

The results of the XANES curve fitting analyses are summarized in detail in Figure 3 (pre-edge amplitude removal) and Figure 4 (negative edge shifts). The amounts of TcO_4^- reduction indicated by the pre-edge amplitudes and absorption edge shifts are in close agreement. This agreement verifies the methodology of the deconvolution technique for detecting Tc reduction. Mix 1 (OPC) has little or no effect on the reduction of TcO_4^-, regardless of temperature or curing duration. Mixes 2 and 3, which contain the BFS additive, produce partial reduction upon going to

higher curing temperatures. Despite the different BFS and PFA compositions in Mixes 2 and 3 at 60°C, the extent of reduction without FeS in these mixtures appears to be similar. With the exception of Mix 2 at 60°C, the addition of FeS results in an increase in TcO_4^- reduction at both low and high temperatures. However, one interesting observation is that the combination of components in Mix 2 appears to inhibit the reduction of TcO_4^- by the added FeS relative to the components in Mix 3. One possible cause of this effect is that the presence of PFA in Mix 2, which reduces cement permeability, may also hinder the accessibility of FeS to the TcO_4^-. There is also a reverse trend which is most apparent in the Mix 3 HT series, in which longer curing times result in less reduction. We attribute this to re-oxidation during the course of the experiment due to diffusion of oxygen into the small experimental samples after reduction of the TcO_4^-.

In Figure 5, we show the Tc K-edge XANES spectra for the Tc cement mixtures prepared in the second stage of the study. Both of the additives FeS and Na_2S have a similar effect, completely reducing the TcO_4^-, as shown by the lack of the $1s \rightarrow 4d$ pre-edge signature. On the other hand, little or no reduction occurred when FeO, Fe_3O_4, or Mn_3O_4 were added. These results suggest that sulfide containing species are important for the reduction of TcO_4^- in these cement matrices. This result is consistent with earlier studies which found decreased Tc leaching in the presence of sulfide species [8]. For comparison, a BFS-treated sample with no added PFA is also shown in Figure 5d. Consistent with the BFS-PFA sample shown earlier in Figure 2b, this sample has a residual amount of TcO_4^- indicating only partial reduction. From the lack of a significant pre-edge feature in Figure 5c, it is apparent that NaH_2PO_2 is quite effective at achieving reduction of the TcO_4^-. However, a comparison with the XANES spectra of the sulfide treated cements shows differences in the fine structure and position of the NaH_2PO_2-treated sample absorption edge. This result indicates that the NaH_2PO_2 reduced species has a coordination environment which is different than that produced by the S-containing additives.

2. EXAFS.

It is instructive to examine the EXAFS spectra of the model compounds to facilitate the interpretation of the cement spectra. We have presented an EXAFS analysis for TcO_2 in a previous

report [24]. Tc EXAFS results for (n-Bu_4N)[$TcOCl_4$] and (n-Bu_4N)$_2$[$TcCl_6$] have been published by Thomas et al. [31]. However, this work does not present the raw EXAFS or FTs to provide a visual comparison with our present study. The raw k^3-weighted EXAFS spectra and Fourier transform (FT) magnitudes for NH_4TcO_4 (aq), NH_4TcOCl_4, and $(NH_4)_2TcCl_6$ and the corresponding curve-fits are presented in Figure 6. The FT magnitudes represent a pseudo-radial distribution function of the near-neighbors present around the central Tc. Due to the backscattering phase shifts which are different for each neighboring atom (α=0.2-0.5 Å), the FT peaks appear at lower R values relative to the true near neighbor distances. The EXAFS spectra of NH_4TcO_4 (aq) and $(NH_4)_2TcCl_6$ are dominated by single frequency patterns that arise from backscattering of well-ordered O (at 1.72 Å) or Cl (at 2.35 Å) shells around the Tc atom. The EXAFS and FT spectra of NH_4TcOCl_4 show a more complex pattern which is composed of a single oxygen atom at 1.63 Å (shorter than the Tc–O bonds in TcO_4^-) and four Cl atoms at 2.32 Å. In all cases, the bond lengths and coordination numbers derived from the EXAFS curve fits (Table 2) are in close agreement with the XRD values and previous EXAFS results [31]. The lack of significant FT features past the first coordination sphere indicates little or no extended structure in these compounds, which is generally expected for discrete molecular complexes.

A comparison of the EXAFS spectra and FTs for the BFS, Na_2S, and FeS treated cements (Figure 7) with the spectra for the model compounds corroborates the XANES findings, demonstrating that significant removal of TcO_4^- has taken place in the presence of the S-containing additives. The theoretical fits (also shown in Figure 7) and the structural results in Table 2 demonstrate that the EXAFS spectra for the BFS, Na_2S, and FeS treated cements are dominated by backscattering from sulfur near neighbors. Although it is not possible to distinguish S backscatterers from Cl backscatterers solely on the basis of an EXAFS analysis, the presence of S neighbors around the Tc is indicated mechanistically by the direct involvement of sulfide species in BFS, FeS, and Na_2S in the reduction. The BFS-treated sample has ~1 O at 1.69 Å confirming the inference made from the XANES analysis of the presence of a residual amount of TcO_4^- (~25%). Because of averaging effects, the EXAFS spectrum for the BFS-treated sample is similar to that

NH_4TcOCl_4, with the exception that the Tc–O bond length in the BFS sample is more characteristic of Tc-O bonds in TcO_4^- than $TcOCl_4^-$. Unlike the BFS treated sample, the Na_2S and FeS treated cements exhibit a Tc-Tc interaction at ~2.8 Å. The assignment of Tc to this near-neighbor interaction is made on the basis that, apart from the Zr in ZrO_2 which is unreactive, there are no other second-row transition metals present in the cement matrix. Given this observation and the presence of S neighbors at 2.4 Å [32], it is probable that a bridged structure similar to that of TcS_2 (Figure 8a) has been formed. In the FeS-treated FT (Figure 7), the peaks at *ca.* 3.9 and 5.0 Å longer range may indeed reflect the presence of extended structure. Although these peaks were fit reasonably well with Tc neighbors at 4.2 and 5.4 Å, this assignment will require confirmation by experimental data with better signal to noise statistics.

The EXAFS spectra and FTs of the NaH_2PO_2 treated cement (Figure 9) demonstrate a structural pattern that is different from the sulfide reduced samples. There are two major peaks in the FT, and they are shifted to lower R values than the FT peaks in the sulfide reduced samples. The curve fitting results (Table 2) indicate a local environment of O and Tc near neighbors at ~2.0 Å and 2.6 Å, respectively. The Tc-O bonds lengths are in close agreement with those in TcO_2 (Table 2), which also confirms the XANES finding of no residual TcO_4^-. Additionally, it is instructive to compare the EXAFS data for the NaH_2PO_2 treated cement with the data for the LiOH-treated model (Figure 9). There is a pronounced similarity both in the spectral signatures and the metrical parameters derived from the curve-fits, which demonstrate the presence of an oxygen bridged structure analogous to the structure of TcO_2 (Figure 8b). This result is not surprising with respect to the LiOH-treated sample since it is an intermediate species obtained during the synthesis of TcO_2. The strong similarities between the spectra in 9a and 9b serve to corroborate the TcO_2-like structure in the NaH_2PO_2 treated cement.

It is possible to extend the interpretation of these data further by combining the XANES and EXAFS results. Figure 10 shows the Tc K-edge XANES for the Na_2S-treated cement, $(NH_4)_2TcCl_6$, and NH_4TcO_4, and the Re L_1-edge XANES for ReS_2, and $HReO_4$ (aq). The spectra have been aligned to a relative energy scale by setting the $1s \rightarrow 4d$ and $2s \rightarrow 5d$ pre-edge

peak positions for Tc and Re, respectively, to zero. Since the XANES region contains bound state transitions and scattering features whose amplitudes are highly dependent on the local structure, the XANES region may be used to fingerprint specific structural features among chemically similar compounds [33]. This is true for the d^0 oxo-anions, ReO_4^- and TcO_4^-, where apart from slight differences in core-hole line-broadening, the K and L_1-edge spectra of these tetrahedral species appear to be identical.

ReS_2 and TcS_2 are isomorphous [25] with the metal atoms residing in distorted octahedra surrounded by S near neighbors. Since the Na_2S-treated cement has Tc–S bond lengths similar to the Tc–X (X=S, Cl) bond lengths in TcS_2 and $TcCl_6^{2-}$, its XANES spectrum can be analyzed using the $(NH_4)_2TcCl_6$ and ReS_2 spectra as references for symmetric and distorted TcS_6 octahedra, respectively. Three distinct peaks lying immediately above the main absorption edge are observed in the $(NH_4)_2TcCl_6$ spectrum. Moving to the Na_2S-treated cement and ReS_2 spectra, the peaks as well as the main absorption edges are broadened and less pronounced. Preliminary modeling of the $(NH_4)_2TcCl_6$ and ReS_2 XANES with FEFF6 indicates that these resonances arise from EXAFS scattering and that the broadening observed in the ReS_2 spectrum results from disorder. Since the Na_2S-treated cement XANES corresponds closely with that of ReS_2, both of which are broadened relative to the $(NH_4)_2TcCl_6$ spectrum, these results suggest that the Tc environment in the Na_2S-treated cement is a disordered array of S atoms. The larger Debye-Waller factor (i.e., greater disorder) in Table 2 for the Na_2S treated sample relative to $(NH_4)_2TcCl_6$ is consistent with this assignment.

Conclusion

We have shown that XANES and EXAFS can be utilized to quantitatively determine changes in the oxidation state and local structure of Tc in cement waste forms. While the addition of BFS achieves only partial reduction under the conditions described here, addition of pure Na_2S and FeS reduced the TcO_4^- completely. These observations, combined with the absence of reduction by FeO, Fe_3O_4, and Mn_3O_4, suggest that a sulfide containing species is the active

reducing agent in BFS. This is consistent with results from previous studies [8]. In all cases where sulfide has been utilized, the reduced Tc species has Tc–S bonds. For the Na_2S and FeS additives, Tc–Tc interactions are observed giving rise to an oligomeric structure such as is found in TcS_2. Other reducing agents such as NaH_2PO_2 are also effective in reducing TcO_4^-, where the reduced species formed resembles TcO_2.

These results demonstrate the utility of XANES and EXAFS in evaluating the efficacy of different cement formulations in reducing the TcO_4^- anion. In addition, it is possible to determine the Tc speciation under a given set of waste form preparation conditions. In this work, we showed that either TcS_2 or TcO_2-like species could be formed, depending on the cement formulation employed. This information together with measurements on properties such as phase stability and solubility may be used to assist efforts aimed at obtaining maximum immobilization of the encapsulated radionuclides.

Acknowledgment

This work was supported by the Director, Office of Energy Research, Office of Basic Energy Sciences, Chemical Sciences Division of the U. S. Department of Energy under contract No. DE-AC03-76SF00098 and by Lawrence Livermore National Laboratory under contract No. W-7405-ENG-48. This work was done at SSRL which is operated by the Department of Energy, Division of Chemical Sciences.

References

1. Glasser, F. P., Atkins, M.: Cements in Radioactive Waste Disposal. MRS Bull. Vol. 19, no.12 , 33-38 (1994).
2. Huang, F. H., Mitchell, D. E., Conner, J. M.: Low-level Radioactive Hanford Wastes Immobilized by Cement-Based Grouts. Nucl. Technol. **107**, 254-270 (1994).
3. Atabek, R., Bouniol, P., Vitorge, P., Le Bescop, P., Hoorelbeke, J. M.: Cement Use for Radioactive Waste Embedding and Disposal Purposes. Cem. Concr. Res. **22**, 419-429 (1992).
4. Plecas, I. B., Peric, A. D., Drljaca, J. D., Lostadonovic, A. M., Glodic, S. D.: Immobilization of Radioactive Waste Water Residues in a Cement Matrix. Cem. Concr. Res. **22**, 571-576 (1992).
5. Xuequan, W., Yen, S., Xiaodong, S., Mingshu, T., Liji, Y.: Alkali-Activated Slag Cement Based Radioactive Waste Forms. Cem. Concr. Res. **21**, 16-20 (1991).
6. Lee, D.L., Fenton, A.: The Development of Cement Formulations for Radioactive Waste Encapsulation. Hazardous Wastes in *Stabilization and Solidification of Hazardous, Radioactive, and Mixed Wastes, 2nd Volume,* T. M. Gilliam and C. C. Wiles, Eds., ASTM, Philadelphia, 348-358 (1992).
7. (a) Langton, C. A.: Challenging Applications for Hydrated and Chemically Reacted Ceramics. DP-MS-88-163 (1988); (b) Langton, C. A.: Slag-Based Materials for Toxic Metal and Radioactive Waste Stabilization. DP-MS-87-95 (1987).
8. Gilliam, T. M., Spence, R. D., Bostick, W. D., Shoemaker, J. L.: Solidification /Stabilization of Technetium in Cement-Based Grouts. J. Hazard. Mater. **24**, 189-197 (1990).
9. Lee, P. A., Cirin, P. H., Eisenberger, P., Kincaid, B. M.: Extended X-ray Absorption Fine Structure-Its Strengths and Limitations as a Structural Tool. Rev. Mod. Phys. **53**, 769-806 (1981).

10. Brown, G. E. Jr., Calas, G., Waychunas, G. A., Petiau, J.: X-ray Absorption Spectroscopy: Applications in Mineralogy and Geochemistry. In: Reviews in Mineralogy, (F. C. Hawthorne, ed.) Mineralogical Society of America, Vol. 18, 431-512 (1988).

11. Shuh, D. K., Kaltsoyannis, N., Bucher, J. J., Edelstein, N. M., Clark, S. B., Nitsche, H., Reich, T., Hudson, E. A., Almahamid, I., Torretto, P., Lukens, W., Roberts, K., Yee, B. C., Carlson, D. E., A. Yee, Buchanan, B. B., Leighton, T., Yang, W.-S., Bryan, J. C.: Environmental Applications of XANES: Speciation of Tc In Cement After Chemical Treatment and Se After Bacterial Uptake. MRS Symp. Proc. **344**, 323-328 (1994).

12. Lee, J. F., Bajt, S., Clark, S. B., Lamble, G. M., Langton, C. A., Oji, L.: Chromium Speciation in Hazardous, Cement-based Waste Forms. Physica B **208/209**, 577-578 (1995).

13. Colton, R., Tomkins, I. B.: Halides and Oxide Halides of Technetium. Aust. J. Chem. **21**, 1981 (1968).

14. Davison, A., Trop, H. S., Depamphilis, B. V., Jones, A. G.: Inorganic Synthesis Vol. **21** Ed. J. P. Fackler, John Wiley and Sons, Inc., New York, 160-162 (1982).

15. Dalziel, J., Naida S. G., Nyholm, R. S., Peacock, R. D.: Technetium. Part I. The Preparation and Properties of Potassium Hexahalogenotechnates. J. Chem. Soc. 4012-4016 (1958).

16. JCPDS-ICDD, Powder Diffraction File. Alphabetical index. Inorganic Phases. Diffraction card no. 24-922 (1993).

17. Bajt, S., Clark, S. B., Sutton, S. R., Rivers, M. L., Smith, J. V.: Synchrotron X-ray Microprobe Determination of Chromate Content using X-ray Absorption Near-Edge Structure. Anal. Chem. **65**, 1800 (1993).

18. Iida, A; Noma, T.: Correction Of The Self-Absorption Effect In Fluorescence X-Ray Absorption Fine Structure. Jap. J. Appl. Phys. Part 1 **32**, 2899-2902 (1993).

19. *X-ray Absorption: Principles, Applications, Techniques for EXAFS, SEXAFS, and XANES*, Eds. Prins, R., Koningsberger, D. E. Wiley-Interscience: New York, (1988).

20. Rehr, J. J., Mustre de Leon, J., Zabinsky, S., Albers, R. C.: Ab-initio Curved Wave X-ray Absorption Fine Structure. Phys. Rev. B **44**, 4146 (1991).

21. Krebs, B., Hasse, K.-D.: Refinements of the Crystal Structures of $KTcO_4$, $KReO_4$, OsO_4. The Bond Lengths in Tetrahedral Oxo-anions and Oxides of d^0 Transition Metals. Acta Crystallogr., Sect. B **32**, 1334 (1976).

22. Cotton, F. A., Davison, A., Day, V. W., Gage, L. D., Trop, H. S.: Preparation and Structural Characterization of Salts of Oxotetrachlorotechnetium(V). Inorg. Chem. **18**, 3024-3029 (1979).

23. Elder, R. C., Estes, G. W., Deutsch, E.: Ammonium Hexachlorotechnetate (IV). Acta Crystallogr., Sect. B **35**, 136-137 (1979).

24. Almahamid, I., Bryan, J. C., Bucher, J. J., Burrell, A. K., Edelstein, N. M., Hudson, E. A., Kaltsoyannis, N., Lukens, W., Nitsche, H., Reich, T., Shuh, D. K.: Electronic and Structural Investigations of Technetium Compounds by X-ray Absorption Spectroscopy Inorg. Chem. **34**, 193-198 (1995).

25. Wildervanck, J. C., Jellinek, F.: The Dichalcogenides of Technetium and Rhenium. J. Less-Common Met. **24**, 73-81 (1971).

26. Wong, J., Lytle, F. W., Messmer, R. P., Maylotte, D. H.: K-edge Absorption Spectra of Selected Vanadium Compounds. Phys. Rev. B **30**, 5596-5610 (1984).

27. Shulman, R. G., Yafet, Y., Eisenberger, P., Blumberg, W. E.: Observation and Interpretation of X-ray Absorption Edges in Iron Compounds and Proteins. Proc. Natl. Acad. Sci., U.S.A. **73**, 1384-1388 (1976).

28. Srivastava, U. C., Nigam, H. L. X-ray Absorption Edge Spectrometry (XAES) as Applied to Coordination Chemistry. Coord. Chem. Rev. **9**, 275-310 (1972).

29. The -12 eV shift in the edge energy of Tc metal relative to TcO_4^- is a correction to the -20 eV shift reported by reference 24, in which the metal spectrum was not adjusted for self-absorption.

30. Elder, R. C., Eidsness, M. K.: Synchrotron X-ray Studies of Metal-Based Drugs and Metabolites. Chem. Rev. **87**, 1027-1046 (1987).

31. Thomas, R. W., Heeg, M. J., Elder, R. C., Deutsch, E.: Structural (EXAFS) and Solution Equilibrium Studies on the Oxotechnetium (V) Complexes $TcOX_4^-$ and $TcOX_5^{2-}$ (X=Cl, Br). Inorg. Chem. **24**, 1472-1477 (1985).

32. The bond lengths determined by EXAFS will be averaged when the separation between shells of identical neighbors falls below the theoretical resolution, $\Delta R=\pi/2(k_{max})$. For the Tc cement data presented here, ΔR~0.12 Å.

33. Knapp, G. S., Veal, B. W., Pan, H. K., Klippert, T.: XANES Study of 3d Oxides: Dependence on Crystal Structure. Solid State Comm. **44**, 1343-1345 (1982).

Figure Captions

Figure 1. Normalized Tc K-edge XANES spectra of Tc model compounds: (a) Tc metal, (b) $(NH_4)_2TcCl_6$, (c) TcO_2, (d) LiOH-treated (e) NH_4TcOCl_4, and (f) NH_4TcO_4 (aq).

Figure 2. Normalized Tc K-edge XANES spectra for TcO_4^- in (a) Mix 3 + FeS cured at 60°C for 15 days; (b) Mix 2 cured at 60°C for 7 days; and (c) Mix 1 cured at 60°C for 1 day. The deconvolution of the pre-edge transition (1) and the main absorption edge (2) are shown.

Figure 3. Percentage of TcO_4^- removed in cement mixtures calculated by comparing the amplitude of the XANES pre-edge transition relative to that of pure TcO_4^-. LT=20°C, HT=60°C.

Figure 4. Relative amount of TcO_4^- removed calculated by fitting the position of the Tc XANES main absorption edge relative to that of pure TcO_4^-. LT=20°C, HT=60°C.

Figure 5. Normalized Tc K-edge XANES spectra of TcO_4^-/OPC mixtures cured at 60°C for 4 days in the presence of the reducing agents (a) FeS, (b) Na_2S, (c) NaH_2PO_2, (d) BFS, and (e) Mn_3O_4 (no reaction).

Figure 6. Raw k^3-weighted EXAFS spectra and the corresponding Fourier transforms of experimental data (—) and the best theoretical fits (····) for (a) NH_4TcO_4 (aq), (b) NH_4TcOCl_4, and (c) $(NH_4)_2TcCl_6$.

Figure 7. Raw k^3-weighted EXAFS spectra and the corresponding Fourier transforms of experimental data (—) and the best theoretical fits (····) for (a) BFS, (b) Na_2S, and (c) FeS treated cements.

Figure 8. Tc structures which exhibit the type of bridging that occurs in the Na_2S, FeS and NaH_2PO_2 treated cements, respectively: (a) TcS_2, and (b) TcO_2. The shaded atoms are S and O.

Figure 9. Raw k^3-weighted EXAFS spectra and the corresponding Fourier transforms of experimental data (—) and the best theoretical fits (····) for (a) NaH_2PO_2 treated cement and (b) LiOH-treated Tc model.

Figure 10. Normalized XANES spectra for (a) ReS_2, (b) Na_2S treated cement, (c) $(NH_4)_2TcCl_6$, (d) $HReO_4$ (aq), and (e) NH_4TcO_4 (aq). The rhenium spectra were measured at the Re L_1-edge and aligned on a relative energy scale with the Tc K-edge spectra.

Table 1. Compositions of Cement Mixtures

	SWS	BFS	PFA	OPC
Mix 1	50%			50%
Mix 2		23%	23%	4%
Mix 3	50%	50%		

Table 2. EXAFS Structural Parameters for Tc compounds.
Values in brackets are taken from XRD studies noted in the text.

	Tc–O			Tc–Cl (S)			Tc–Tc		
Sample[a]	R(Å)	N[b]	σ^{2c}	R(Å)	N	σ^2	R(Å)	N	σ^2
TcO_4^-	1.72 [1.71]	4.2 [4]	0.0015						
$TcOCl_4^-$	1.63 [1.61]	1.3 [1]	0.0020	2.32 [2.31]	4.5 [4]	0.0027			
$TcCl_6^{2-}$				2.35 [2.35]	5.8 [6]	0.0031			
TcS_2				[2.24-2.55]	[6]		[2.55-2.92]	[3]	
BFS	1.69	0.8	0.0031	2.33	4.1	0.0055			
Na_2S				2.38	4.0	0.0076	2.75	0.9	0.0020
FeS				2.37	5.1	0.0083	2.80	0.8	0.0025
NaH_2PO_2	2.04	3.9	0.0028				2.59	1.2	0.0032
LiOH	2.08	5.3	0.0058				2.63 2.91	1.0 0.8	0.0030 0.0040
TcO_2[d]	1.98 [1.94-2.08]	6 [6]					2.61, 3.10 [2.48, 3.08]	2 [2]	0.0036

a. Principal Tc-containing species, compound, or reducing agent added to TcO_4^-/cement mixture.

b. Coordination number

c. Debye-Waller factor squared ($Å^2$)

d. Data taken from previous EXAFS study in reference 24.

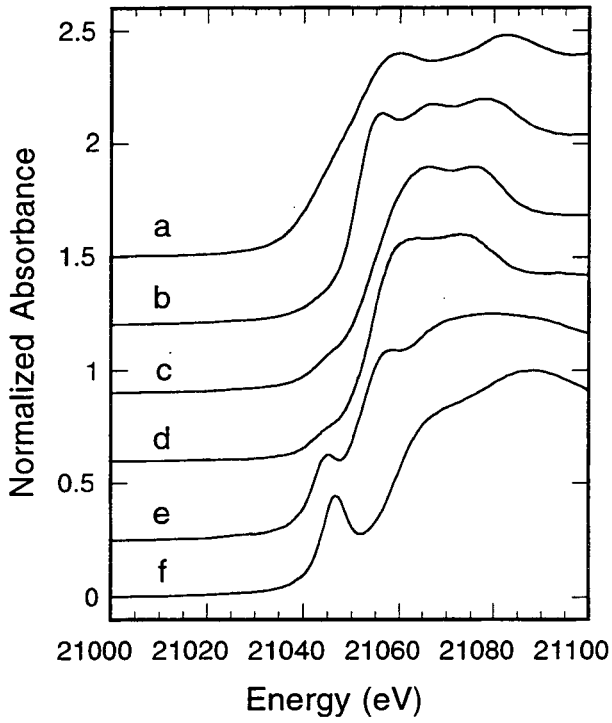
Normalized Absorbance
2.5
2
1.5
1
0.5
0
a
b
c
d
e
f
21000
21020
21040
21060
21080
21100
Energy (eV)

Figure 1

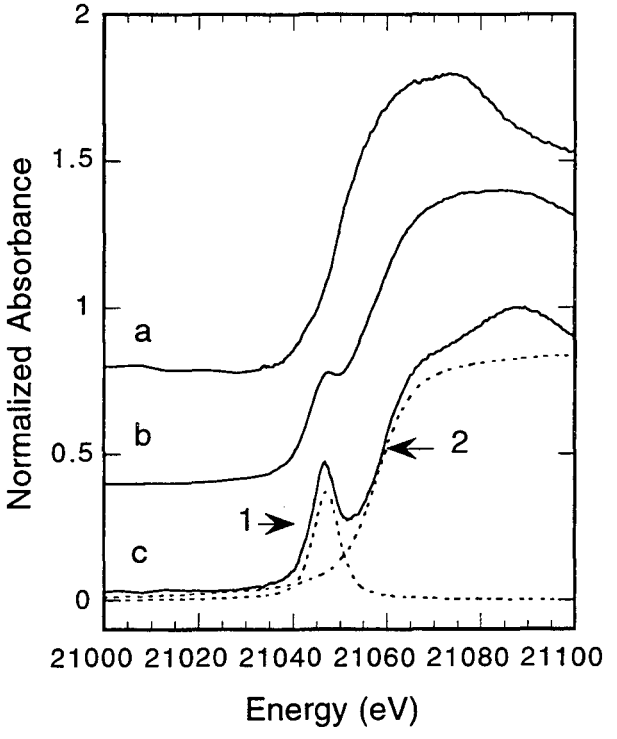
2
1.5
1
0.5
0
Normalized Absorbance
a
b
c
1
2
21000 21020 21040 21060 21080 21100
Energy (eV)

Figure 2

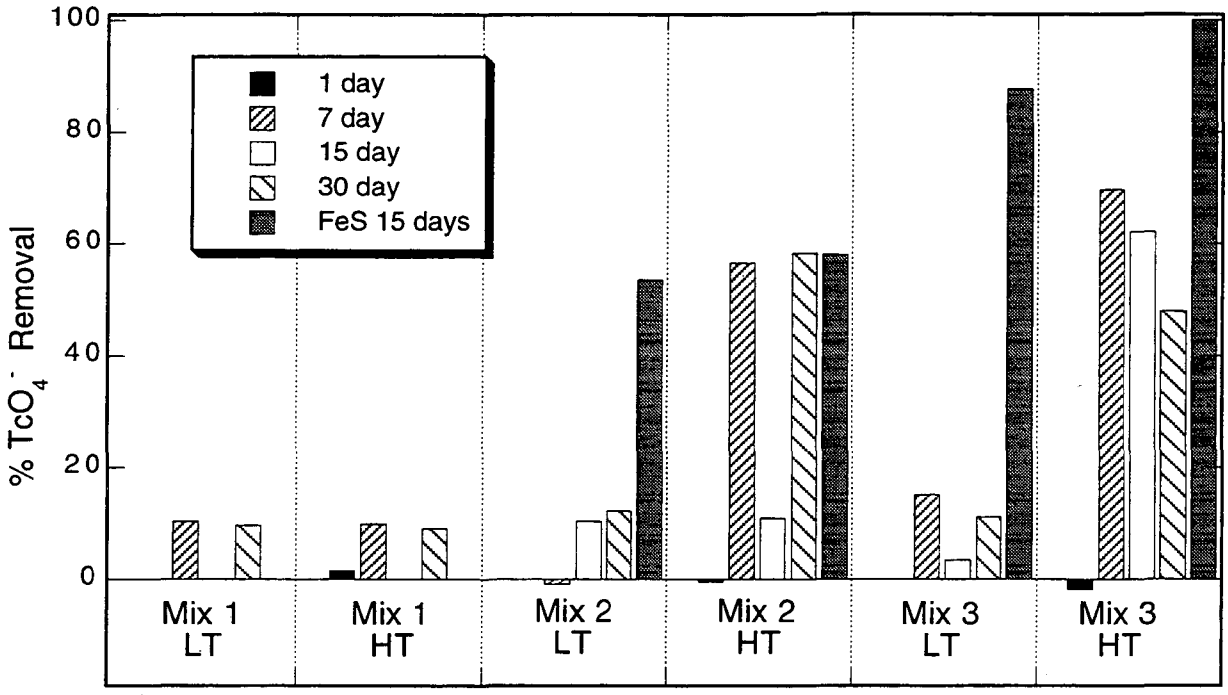
100
80
60
40
20
0
% TcO_4^- Removal
1 day
7 day
15 day
30 day
FeS 15 days
Mix 1 LT
Mix 1 HT
Mix 2 LT
Mix 2 HT
Mix 3 LT
Mix 3 HT

Figure 3

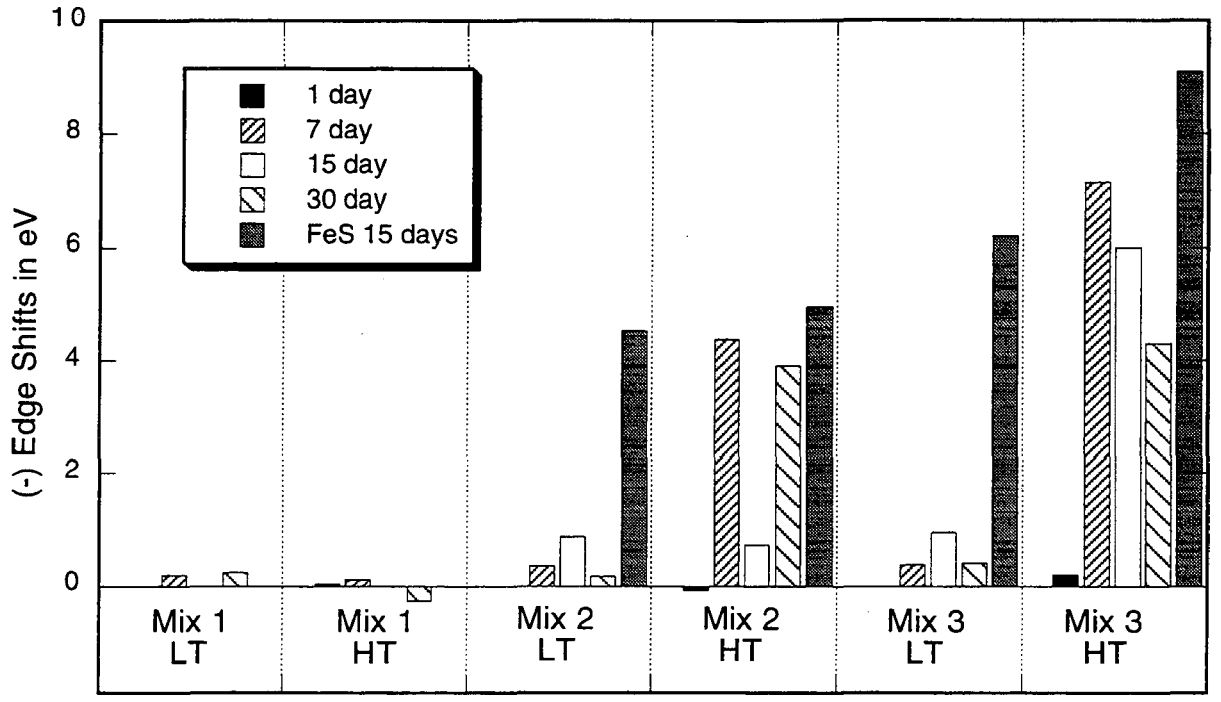
10
8
6
4
2
0
(-) Edge Shifts in eV
1 day
7 day
15 day
30 day
FeS 15 days
Mix 1 LT
Mix 1 HT
Mix 2 LT
Mix 2 HT
Mix 3 LT
Mix 3 HT

Figure 4

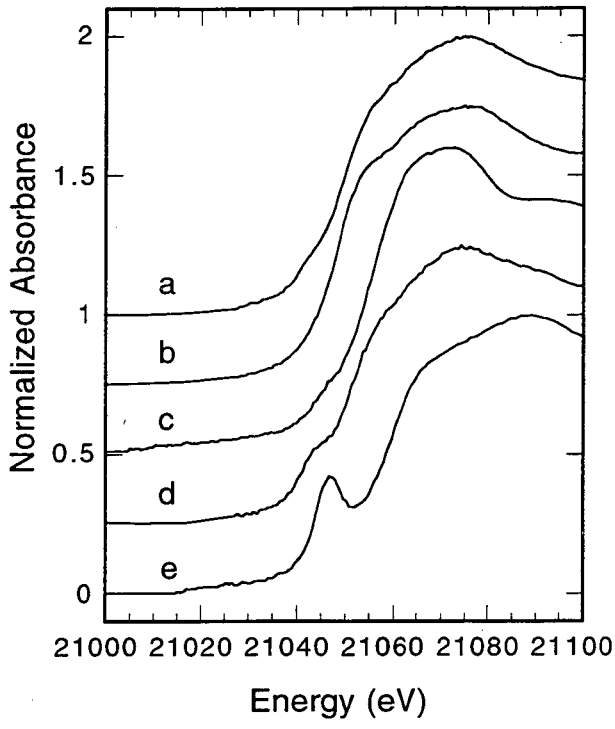
Normalized Absorbance
2
1.5
1
0.5
0
a
b
c
d
e
21000 21020 21040 21060 21080 21100
Energy (eV)

Figure 5

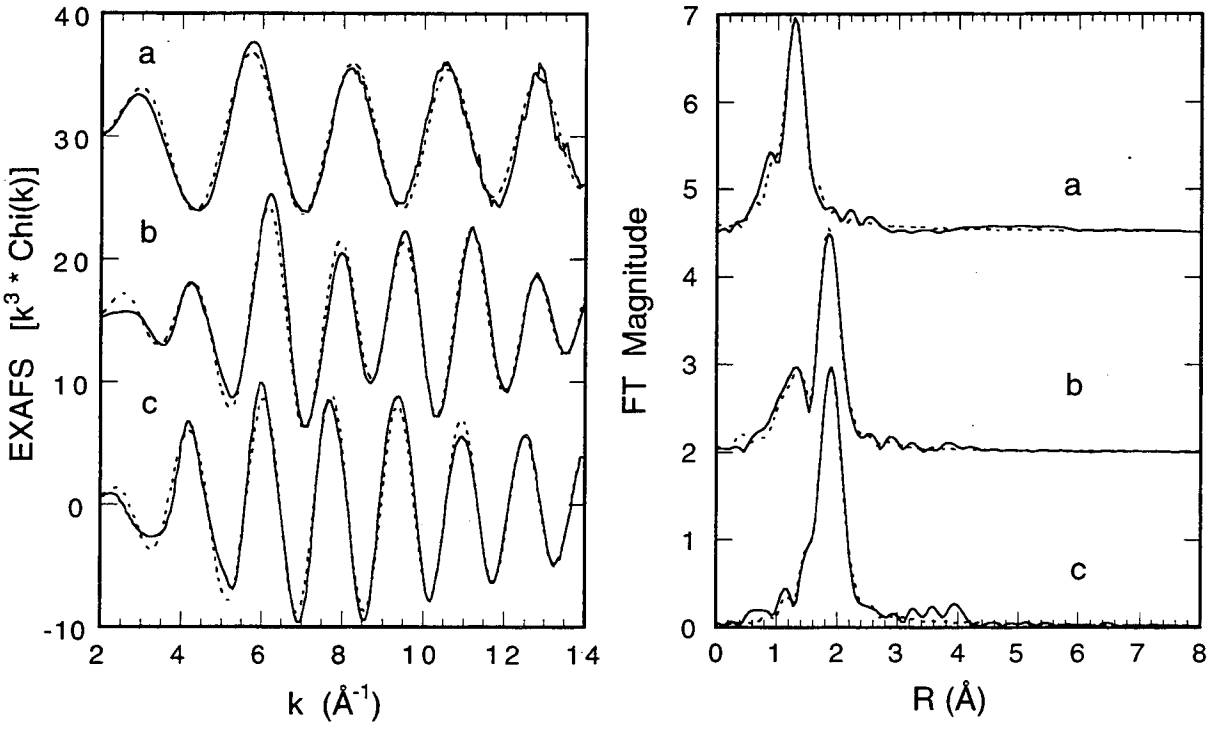

Figure 6

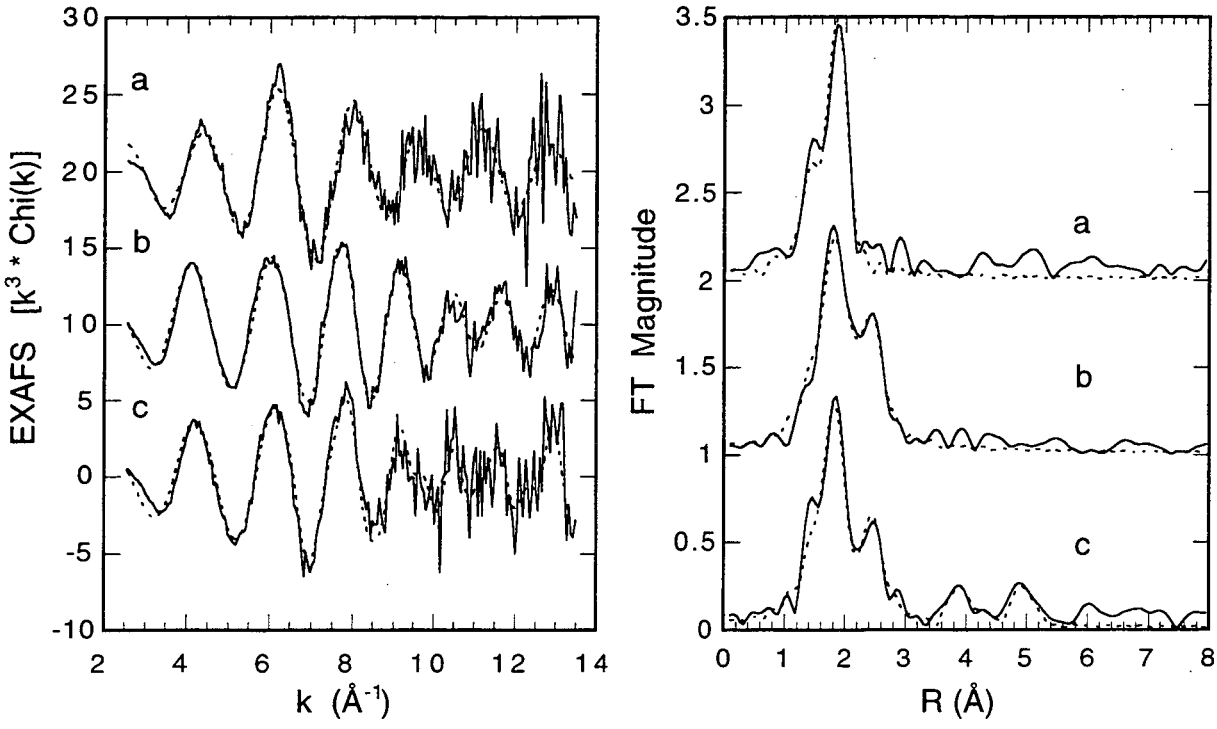

Figure 7

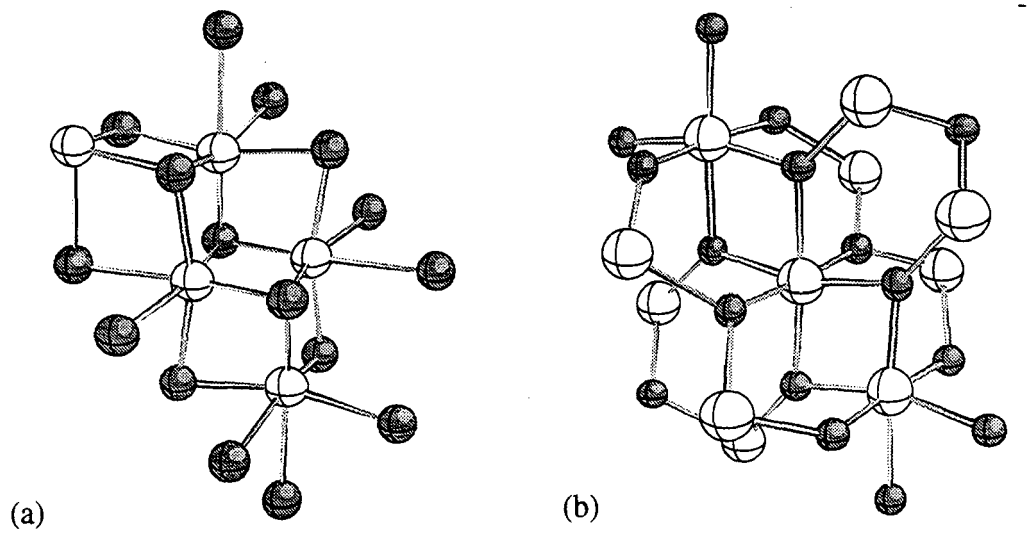

(a) (b)

Figure 8

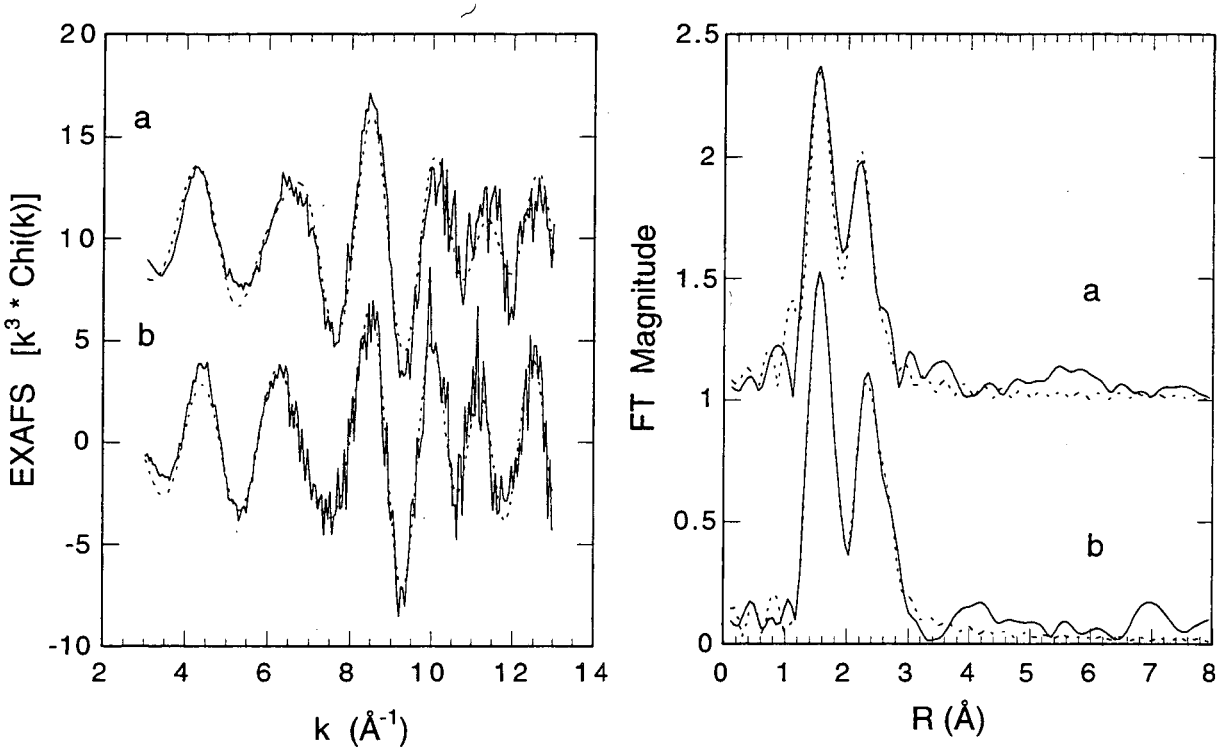

Figure 9

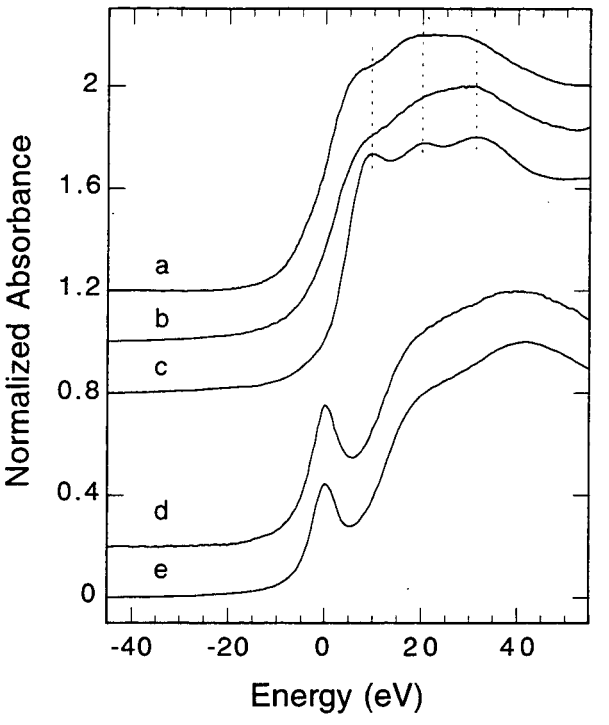
Normalized Absorbance
2
1.6
1.2
0.8
0.4
0
a
b
c
d
e
-40
-20
0
20
40
Energy (eV)

Figure 10

Ernest Orlando Lawrence Berkeley National Laboratory
One Cyclotron Road | Berkeley, California 94720

Prepared for the U.S. Department of Energy under Contract No. DE-AC03-76SF00098